

1 **Microtubule minus-end aster organization is driven by processive HSET-tubulin clusters**

2 Norris et al. (2018)

3 Supplementary Figures 1-7

4

5

6

7

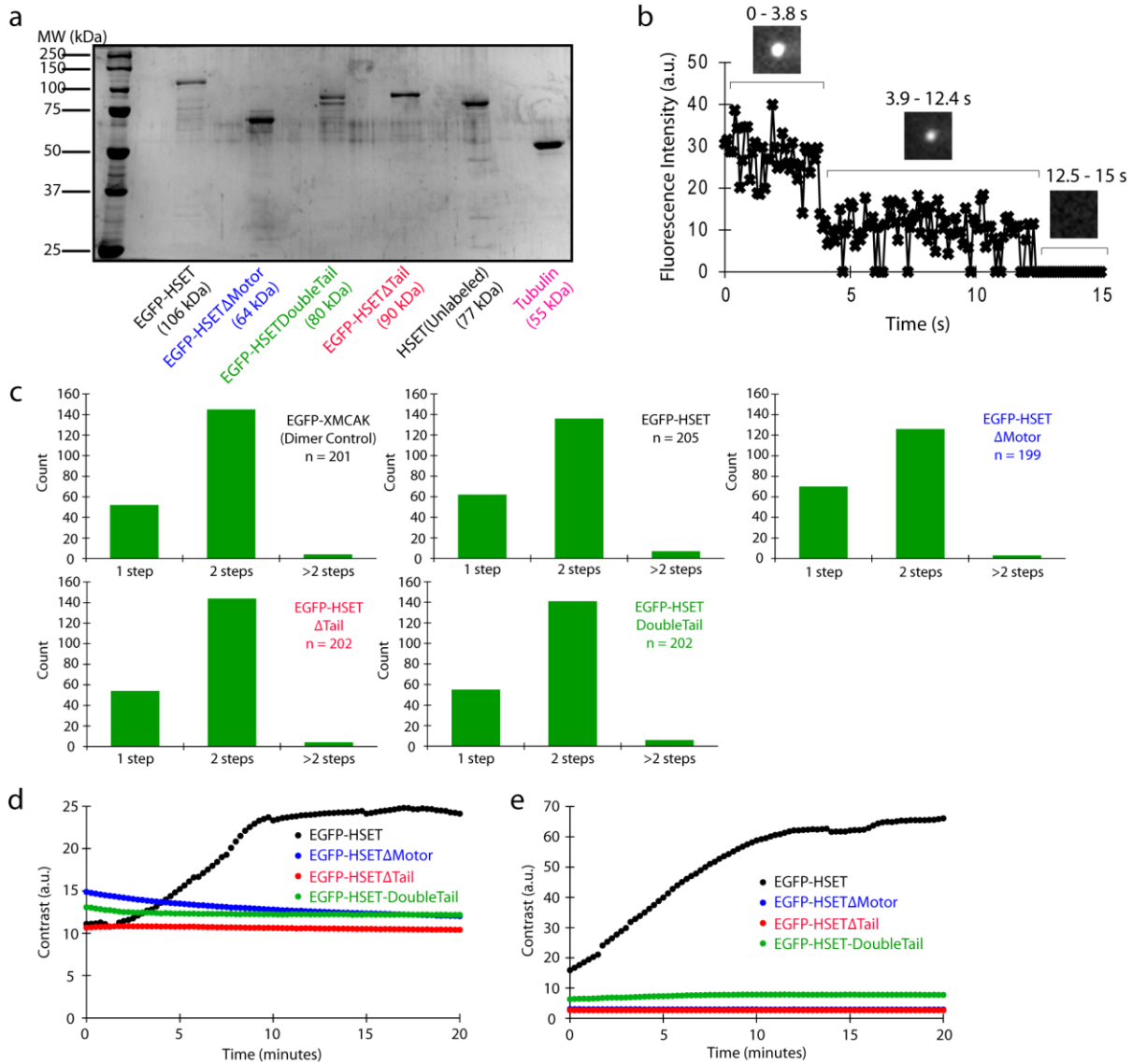
8

9

10

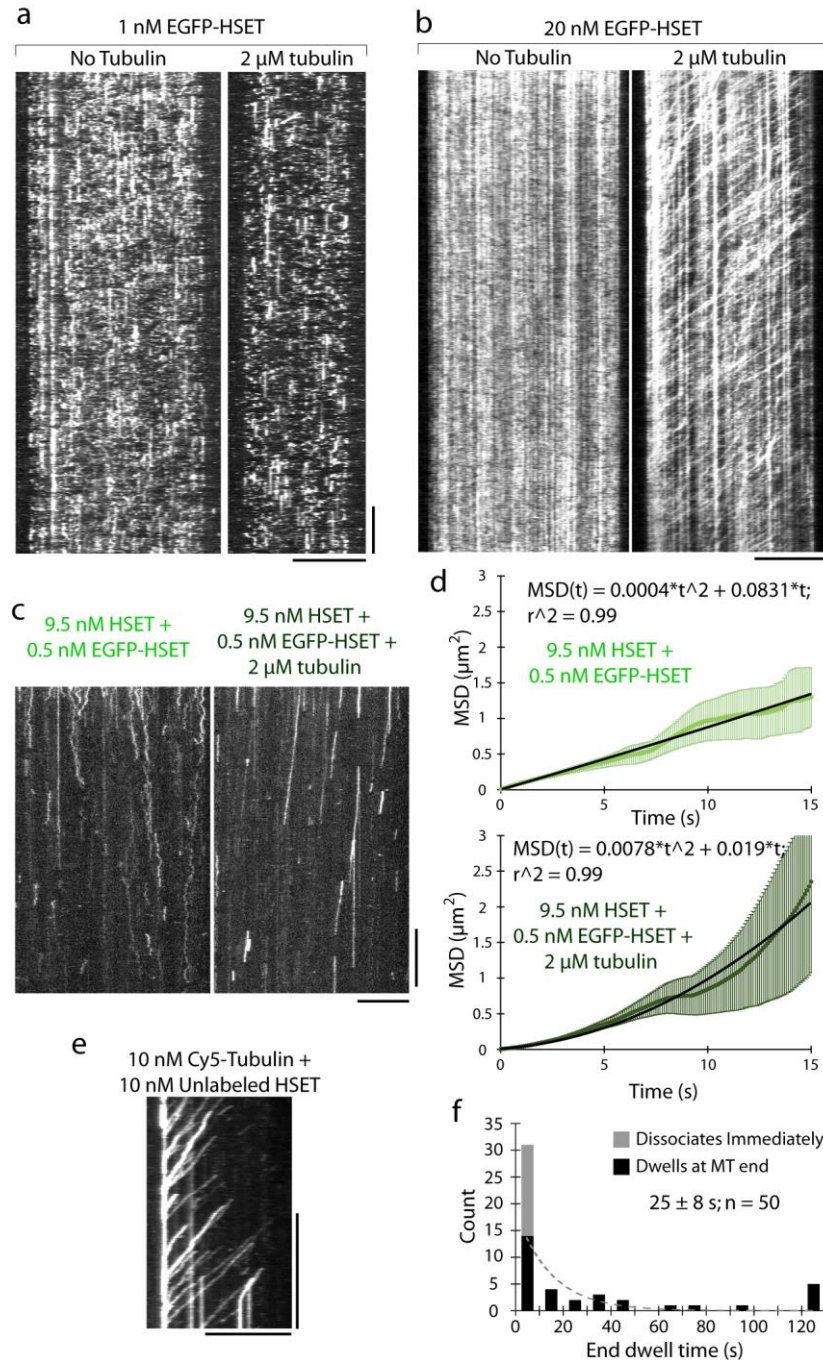
11

12



13

14 **Supplementary Figure 1. Characterization of HSET constructs.** (a) After two-step
 15 purification, 750 ng of the indicated construct was separated by SDS-PAGE and detected by
 16 Coomassie blue. MW markers are indicated on the left, and the predicted MW from the amino
 17 acid sequence for each construct is indicated in parentheses. (b) Representative two-step
 18 photobleaching of EGFP-HSET. EGFP-HSET was diluted to single-molecule concentrations,
 19 adhered to a glass surface, visualized by high-speed TIRF, and the Gaussian intensity was
 20 monitored over time. Insets depict averaged images over the indicated time period for the trace
 21 provided. (c) Quantification of stepwise photobleaching for each construct. The number of
 22 photobleaching steps was quantified for individual molecules and the population data were
 23 plotted as histograms, where the number of particles n from 2 independent experiments is
 24 indicated ($N \geq 4$ movies for each condition). (d) Representative time course of self-organization
 25 (single fields corresponding to (Fig. 1b)) as monitored by contrast (standard deviation) in the
 26 tubulin channel. (e) Representative time course of self-organization (single fields corresponding
 27 to (Fig. 1c)) as monitored by contrast (standard deviation) in the tubulin channel.



28

29 **Supplementary Figure 2. Tubulin activates directed motility of HSET on single MTs. (a-b).**
 30 1 nM (a) or 20 nM (b) EGFP-HSET in BRB80 + 50 mM KCl was monitored by time-lapse TIRF
 31 in the absence (left) or presence (right) of soluble tubulin and visualized by kymograph. Distance
 32 is on the x-axis (scale bar, 10 μ m), and time is on the y-axis (scale bar, 1 min). (c) 10 nM HSET
 33 (5% EGFP-labeled) in P12 buffer was monitored by high-speed time-lapse TIRF in the presence
 34 or absence of 2 μ M tubulin and visualized by kymograph (x-scale bar, distance, 10 μ m; y-scale
 35 bar, time, 10 s). (d) MSD quantification of (a). Data are presented as the calculated mean MSD
 36 (y-axis) from two independent experiments over the indicated time intervals (x-axis), \pm SEM.

37 Solid lines indicate quadratic best fits for the indicated condition, where fits were obtained over
38 the first five seconds with zero origin. Equations and corresponding r^2 values are shown as
39 insets. $n = 215$ particles for $2 \mu\text{M}$ tubulin, $n = 175$ particles for no tubulin. Particles from 2
40 independent experiments are shown, where $N \geq 4$ movies for each condition. **(e)** Representative
41 kymograph of tubulin transport by HSET. Unlabeled HSET (10 nM) was mixed with Cy5-
42 tubulin (10 nM) in BRB80 + 50 mM KCl, monitored by TIRF, and visualized by kymograph (x-
43 scale bar, distance, $10 \mu\text{m}$; y-scale bar, time, 10 s). **(f)** End dwell times for Cy5-tubulin were
44 determined by kymograph analysis and plotted as histograms for the population. Data is reported
45 as the mean values from CDF fitting, \pm the 95% CI from bootstrapping from two independent
46 experiments where $N \geq 4$ movies for each condition. Particles dissociating immediately (<1
47 frame) are color-coded and were excluded from exponential CDF fits.

48

49

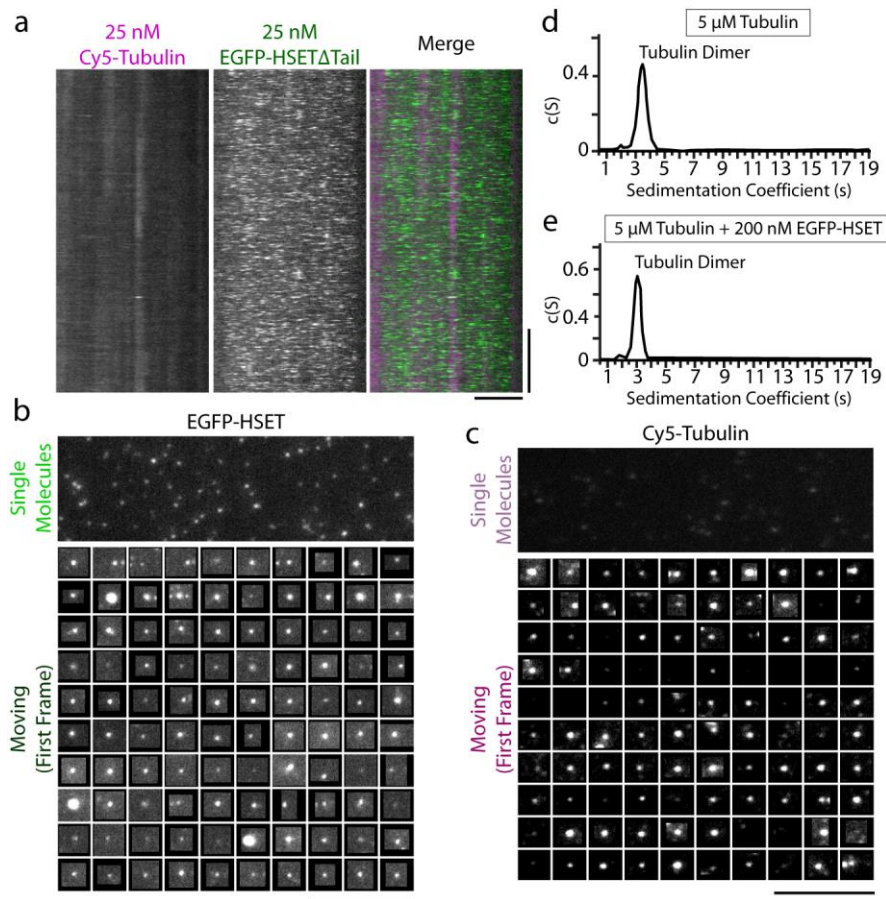
50

51

52

53

54



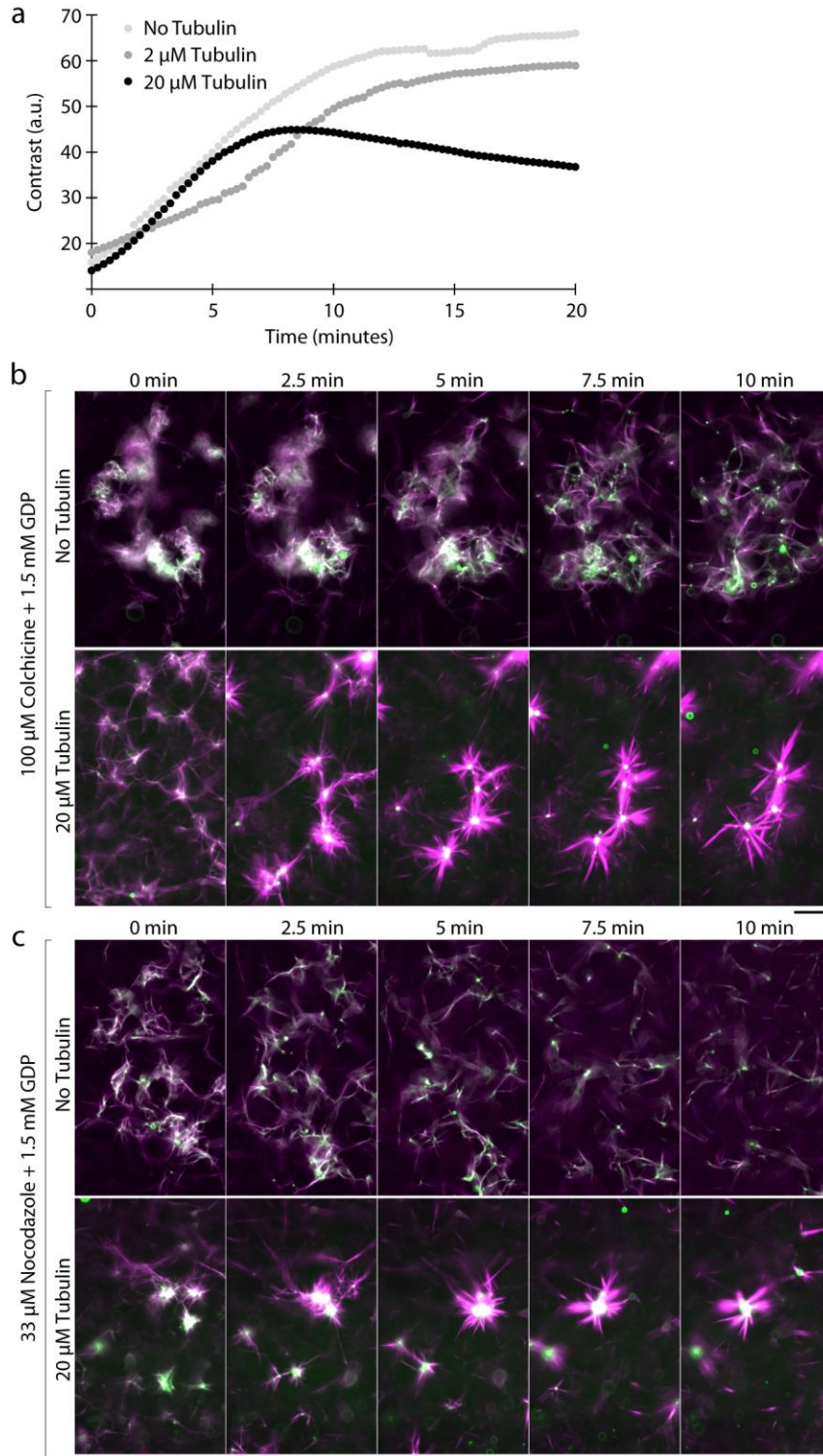
55

56 **Supplementary Figure 3. Tubulin induces HSET clustering upon binding to tail domain.**
 57 (a) Cy5-tubulin (magenta) and EGFP-HSET Δ Tail (green) were mixed in BRB80 + 50 mM KCl,
 58 observed via two-color time-lapse TIRF, and visualized by kymograph at the indicated
 59 concentrations, where EGFP-HSET Δ Tail showed no observable processive motility (x-scale,
 60 distance, 5 μ m; y-scale, time, 1 min). (b) Representative TIRF images of EGFP-HSET diluted to
 61 single-molecule levels and adhered to a glass cover slip (top) compared to the first frame of
 62 moving EGFP-HSET (1 nM) after the addition of 20 μ M tubulin (bottom, n = 100 particles
 63 chosen randomly). Images are processed and acquired identically to illustrate differences in
 64 intensity. Data corresponds to Fig. 3b, top. (c) Representative TIRF images of Cy5-tubulin
 65 diluted to single-molecule levels and adhered to a glass cover slip (top) compared to the first
 66 frame of moving Cy5-tubulin (10 nM) in the presence of 10 nM unlabeled HSET with 1 mM
 67 GTP present (bottom). Images are processed and acquired identically to illustrate differences in
 68 intensity. Data correspond to Fig. 3c. Scale bars, 10 μ m. (d) The sedimentation velocity profile
 69 of 5 μ M tubulin as obtained by sedimentation velocity analytical ultracentrifugation (AUC)
 70 analysis (representative profile). The calculated s [c(s)] is plotted *versus* the sedimentation
 71 coefficient (S), and the profile fit to a continuous sedimentation distribution. The observed
 72 frictional ratio is 1.41 and the r.m.s.d. value is 0.0075. For the prominent peak, $S = 3.397$, which
 73 corresponds to an estimated molecular mass of 102 kDa. (e) The sedimentation velocity profile
 74 of 5 μ M tubulin plus 200 nM EGFP-HSET (representative profile). The observed frictional ratio

75 is 1.57 and the r.m.s.d. value is 0.0091. For the prominent peak, $S = 3.075$, which corresponds to
76 an estimated molecular mass of 80 kDa.

77

78



79

80 **Supplementary Figure 4. Soluble (non-MT) tubulin rescues HSET self-organization**
 81 **independent of polymerization. (a)** Representative time course of self-organization by HSET
 82 upon tubulin addition (single fields corresponding to Fig. 4a) as monitored by contrast (standard
 83 deviation) in the tubulin channel. Unlabeled tubulin concentration is indicated in figure inset. **(b-**

84 **c)** EGFP-HSET driven self-organization of GMPCPP-stabilized MTs in the absence of MT
85 polymerization. Experiments were performed identically to (a) but in the absence of taxol and
86 the presence of saturating colchicine/GDP (b) or nocodazole/GDP (c) to prevent polymerization.
87 Technical replicates of experiments in (b-c) were repeated $n \geq 2$ times for each condition, and
88 representative images are shown. Scale bar, 50 μm .

89

90

91

92

93

94

95

96

97

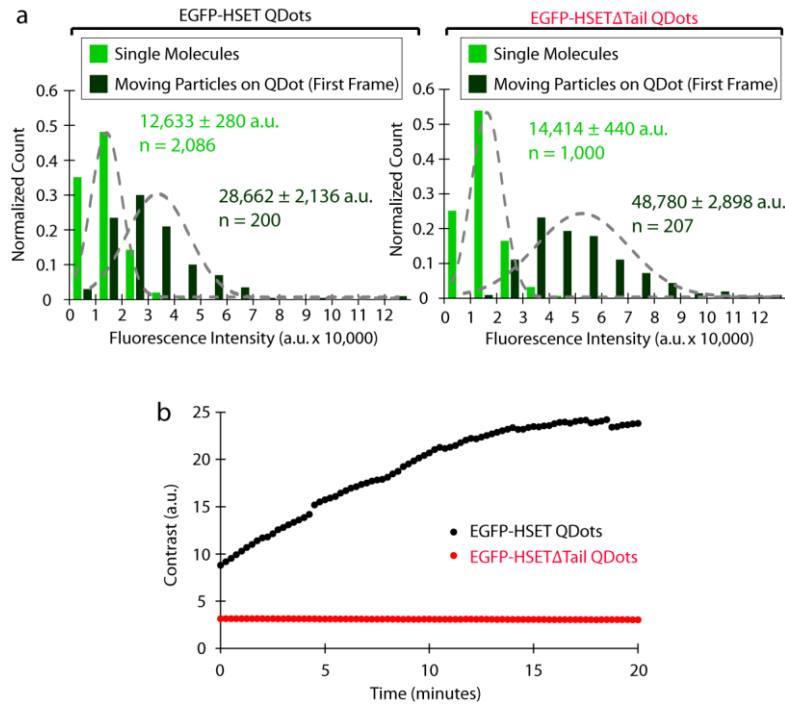
98

99

100

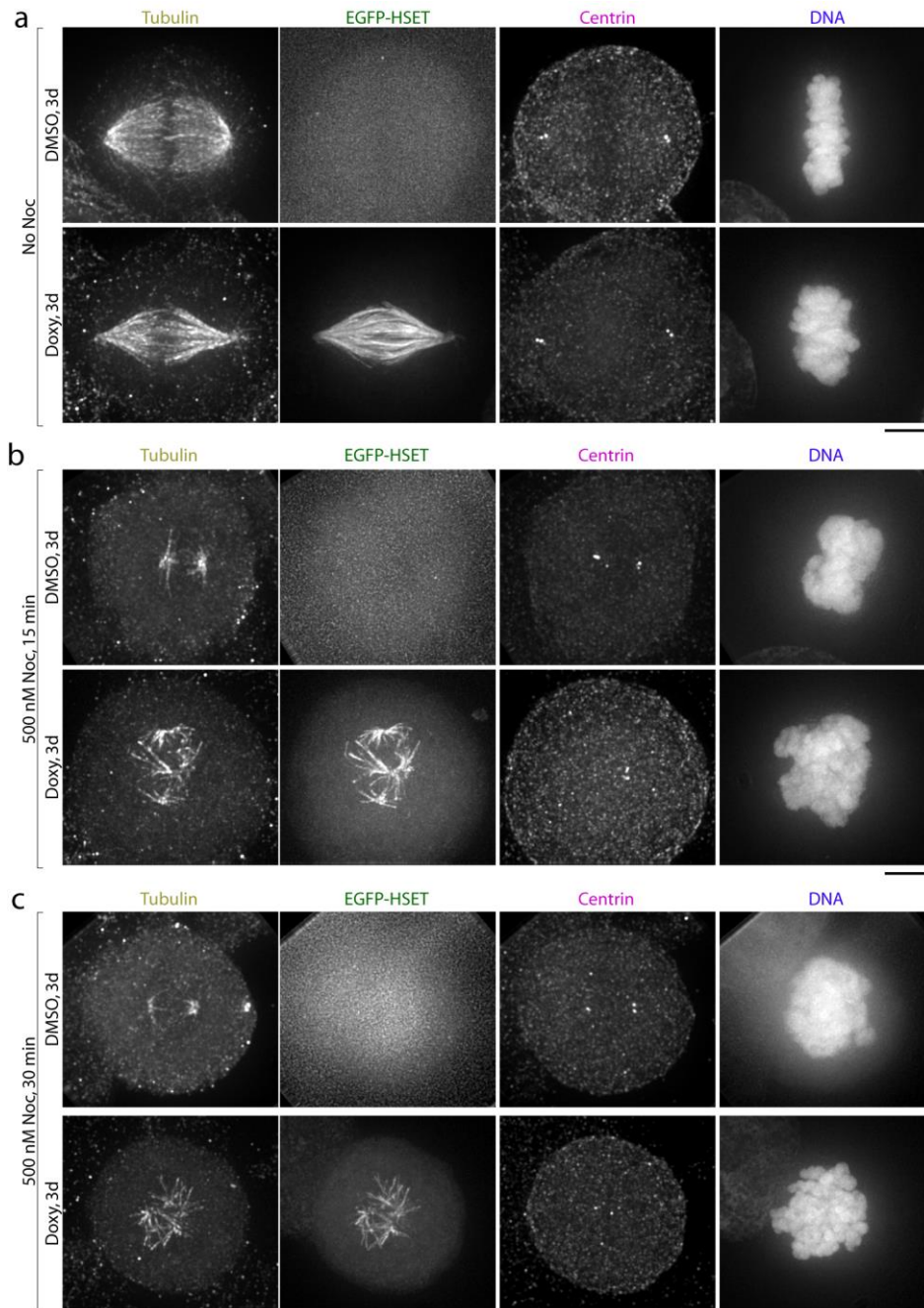
101

102



103

104 **Supplementary Figure 5. Multiple HSET motors conjugated to quantum dots drive aster**
 105 **self-assembly of GMPCPP MTs. (a)** Verification of multi-motor assembly of HSET on QDots.
 106 After EGFP-HSET (left) or EGFP-HSET Δ Tail (right) was conjugated to streptavidin QDots via
 107 the N-terminal 6x-His tag and biotin-anti-His antibody at a 3:1 ratio (see Fig. 5a), these HSET-
 108 QDot complexes were observed by time-lapse TIRF in motility assays. The fluorescence
 109 intensity of the first frame of moving EGFP-HSET particles was determined by Gaussian fit, and
 110 intensity distributions were plotted as histograms for the population (single EGFP-HSET motors,
 111 light green, first frame of moving EGFP-HSET particles, dark green). Data are reported as the
 112 mean intensity values (insets) from CDF fitting to normal distributions, \pm the 95% CI from
 113 bootstrapping from two independent experiments where $N \geq 4$ movies for each condition. Note
 114 that EGFP-HSET-QDots contain less motors per QDot on average; this is likely due to the large
 115 size of the N-terminal tail domain limiting QDot binding. **(b)** Representative time course of self-
 116 organization by HSET-QDot assemblies (single fields corresponding to (Fig. 5e)) as monitored
 117 by contrast (standard deviation) in the tubulin channel. HSET-QDot assembly type is indicated in
 118 figure inset.



119

120 **Supplementary Figure 6. Increasing the relative level of soluble (non-MT) tubulin**
 121 **promotes HSET-driven aster formation in fixed cells.** (a) Spectrally unmixed images
 122 corresponding to Fig. 6b. After pretreating cells for 3d with doxycycline/DMSO, representative
 123 z-stacks of metaphase cells where cells were fixed, then (left to right): immunostained for
 124 tubulin, EGFP-HSET was imaged directly, immunostained for centrin, and stained for DNA
 125 (Hoechst). (b) Spectrally unmixed images corresponding to Fig. 6c. After pretreating cells for 3d
 126 with doxycycline/DMSO then treating cells for 15 min with 500 nM nocodazole, representative
 127 z-stacks of cells where cells were fixed, then (left to right): immunostained for tubulin, EGFP-
 128 HSET was imaged directly, immunostained for centrin, and stained for DNA (Hoechst). (c) After

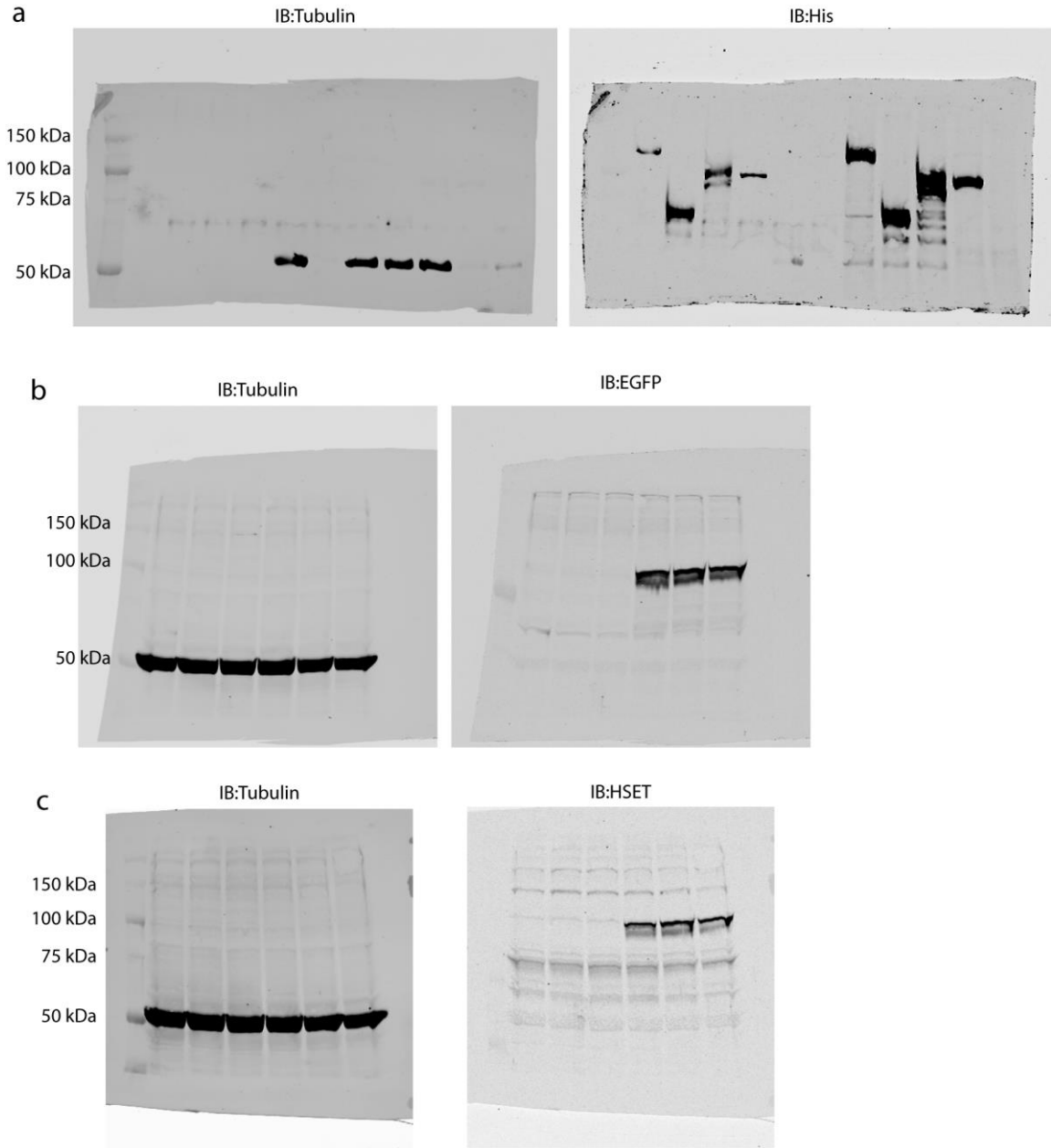
129 pretreating cells for 3d with doxycycline/DMSO then treating cells for 30 min with 500 nM
130 nocodazole, representative z-stacks of cells where cells were fixed, then (left to right):
131 immunostained for tubulin, EGFP-HSET was imaged directly, immunostained for centrin, and
132 stained for DNA (Hoechst). Conditions correspond to Fig. 6d (right), and a representative image
133 is shown. Scale bars, 5 μm .

134

135

136

137



138

139 **Supplementary Figure 7. Full blots corresponding to portions presented in main paper. (a)**
 140 Full blots corresponding to Fig. 3a. **(b)** Full blots corresponding to Fig. 6a, top. **(c)** Full blots
 141 corresponding to Fig. 6a, bottom. See legends in main text for experimental details.